Environ Monit Assess (2009) 152:245–257
DOI 10.1007/s10661-008-0312-8

Vegetation recovery patterns assessment at landslides caused by catastrophic earthquake: A case study in central Taiwan

Wen-Chieh Chou · Wen-Tzu Lin · Chao-Yuan Lin

Received: 15 August 2007 / Accepted: 9 April 2008 / Published online: 5 June 2008

Abstract The catastrophic earthquake, 7.3 on the Richter scale, occurred on September 21, 1999 in Central Taiwan. Much of standing vegetation on slopes was eliminated and massive, scattered landslides were induced at the Jou-Jou Mountain area of the Wu-Chi basin in Nantou County. We evaluated three methods for assessing landslide hazard and vegetation recovery conditions. (1) Self-organizing map (SOM) neural network coupled with fuzzy technique was used to quickly extract the landslide. (2) The NDVI-based vegetation recovery index derived from multi-temporal SPOT satellite images was used to evaluate vegetation recovery rate in the denudation sites. (3) The spatial distribution index (SDI) based on land-cover topographic location was employed to analyze vegetation recovery patterns, including the invading, surviving and mixed patterns at the Jou-Jou Mountain area. On September 27, 1999, there were 849.20 ha of landslide area extracted using the self-organizing map and fuzzy technique combined model. After six years of natural vegetation succession, the landslide has gradually restored, and vegetation recovery rate reached up to 86%. On-site observation shows that many native pioneer plants have invaded onto the denudation sites even if disturbed by several typhoons. Two native surviving plants, *Arundo formosana* Hack and *Pinus taiwanensis* Hayata, play a vital role in natural vegetation succession in this area, especially for the sites on ridgeline and steep slopes.

Keywords Landslide hazard assessment · Vegetation recovery pattern analysis · Self-organizing map (SOM) · Fuzzy technique

W.-C. Chou
Department of Civil Engineering and Engineering Informatics,
Chung Hua University,
Hsinchu City 30012, Taiwan, Republic of China

W.-T. Lin (✉)
Department of Environment and Disaster Management,
Ming Dao University,
369 Wen-Hua Rd., Peetow,
Changhua County 52345, Taiwan, Republic of China
e-mail: aiken@mdu.edu.tw

C.-Y. Lin
Department of Soil and Water Conservation,
National Chung Hsing University,
Taichung City 40227, Taiwan, Republic of China

Introduction

Landslides are very common natural hazards and can be very damaging in steepland areas, resulting in a variety of human and environmental impacts (Perotto-Baldiviezo et al. 2004). On September 21, 1999, a catastrophic earthquake with a Richter magnitude of 7.3 occurred at Chi-Chi area of Nantou County in Taiwan. Massive landslides were induced and more than 20,000 sites, with a total landslide area of 15,977 ha, were identified in Central Taiwan (Chang

2000), including the slopeland along the East–West Expressway in the Da-Chia River basin, in the Jou-Jou Mountain area of the Wu-Chi River basin (Fig. 1), which is located at Tasoling near the border between Yunlin and Chiai counties, and Chiufenershan in Nantou county (Lin et al. 2001). According to the geological data from Taiwan's Central Geological Service, the geology of the study area was chiefly formed by high percentage of gravel, rock and minor sandstone, and the surface was only covered by shallow and fragile topsoil. Therefore, the risk of landslides in the Jou-Jou Mountain area are especially serious.

The Taiwan Forestry Bureau has established a 1198 ha plan for natural reservation purposes at the Jou-Jou Mountain. In accordance with the on-site investigation in this area from Taiwan's Endemic Species Research Institute in September, 2000, the quake significantly affected the ecosystem, including the elimination of habitats for a number of birds and extinction of *Acronychia pedunculata*, a native plant in Taiwan. Ou and Liu (2000) pointed out that without human interference many plants have naturally invaded into the landslide one year after the earthquake and some of surviving plants can quick cover the landslides during rainy seasons.

Succession is a natural process that determines consecutive changes in species composition of the vegetation resulting from developmental changes in the ecosystem itself or initiated by a disturbance (Myster et al. 1997; Roovers et al. 2005). In general, vegetation recovery is generally regarded as a slow process (Brown and Al-Mazrooei 2003), several environmental factors such as soil properties and moisture, slope gradient, typhoon disturbances and microclimate affect the rate of natural vegetation succession.

The scope of such tremendous, scattered landslides and the vegetation recovery could not be assessed using traditional methods, such as field surveys, a

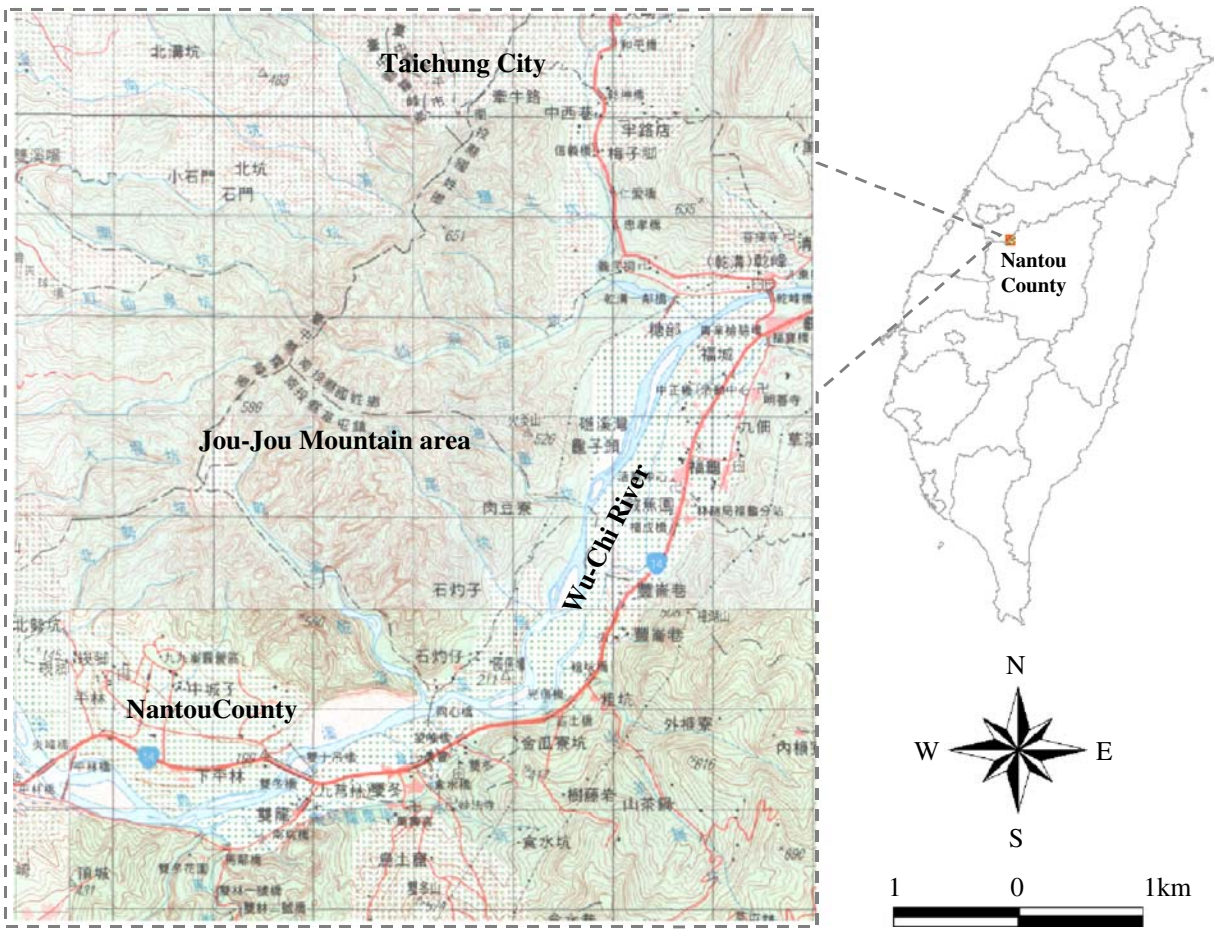

Fig. 1 Jou-Jou Mountain area in Central Taiwan

variety of measuring equipment, or airborne photo interpretation by available manpower. Fast growing progress in technologies including remotely sensed data and digital elevation models (DEMs) coupled with geographic information systems (GIS) are now being widely used for the landslides disaster assessment (Mantovani et al. 1996; Dikau et al. 1996; Carrara et al. 1999; Dhakal et al. 2000; Claessens et al. 2006). The frequently used methods for landslide classification include ISODATA, Minimum Distance, Mahalanobis Distance and Maximum Likelihood Estimation (MLE) and fuzzy *c*-mean algorithms. The fuzzy classifier is an unsupervised classification method, which has proven useful in post-classification processing, the detection of high-risk confusion zones, and the correction of flagrant misclassification (Andrefouet et al. 2000; Keuchel et al. 2003). For temporal and spatial dynamics of vegetation, the normalized difference vegetation index (NDVI) derived from remotely sensed data is a popular method (Teillet et al. 1997; Kumar et al. 2002; Larchevêque et al. 2005). Higher NDVI indicates a greater level of photosynthetic activity (Sellers 1985), which can be used to evaluate the amount of vegetation cover and biomass.

There have been over six years since the earthquake. Most research on the Chi-Chi earthquake-induced landslides mainly focused on the landslide disaster statistics and surveys (Wang et al. 2000; Chang 2000; Wang et al. 2003) and on the vegetation, which has been investigated via field observation or a variety of measuring equipment (Ou and Liu 2000; Lin and Huang 2000).

For massive, scattered landslides, it is essential to develop the quantitative methods coupled with remotely sensed data and GIS for effective the landslide hazard and long-term vegetation recovery conditions assessment for decision making and policy planning. Therefore, three procedures were evaluated in this study. Firstly, self-organizing map (SOM) neural networks coupled with fuzzy techniques were used to identify landslides from pre- and post-quake SPOT images. Secondly, an NDVI-based index, the vegetation cover index (*C*) was derived to assess vegetation recovery conditions at landslides. Finally, three vegetation recovery patterns were analyzed using a spatial distribution index (SDI) based on topographic distribution. Additionally, on-site investigation can be used to verify landslide distributions, to evaluate the characteristics of surviving and invading plants at different patterns, and to monitor the natural rate of vegetation succession on landslide areas.

Study area

The Jou-Jou Mountain area is located at the north shore of the Wu-Chi River in central Taiwan (Fig. 1). The area lies between 20°59′59″ N and 23°59′12″ N latitudes and between 120°44′51″ E and 120°48′12″ E longitudes. The study area is 4,396 ha with altitudes from 123 to 776 m, an average slope of 39% and an average precipitation of 1684 mm/year. The geological data from Taiwan's Central Geological Service shows that the rock formation occurring in the target area is the Tou-Ke-Shan stratification, chiefly formed by high percentage of gravel, rock and minor sandstone. Over time, the slopes adjacent to active stream channels have eroded by torrential water flows from theWu-Chi River. A cliff terrain results from this geomorphic activity. The major grass species and trees are Formosan giantreed, *Arundo formosana* Hack, Taiwan Red Pine, *Pinus taiwanensis* Hayata, and Taiwan Shortleaf Pine, *Pinus morrisonicola* Hayata.

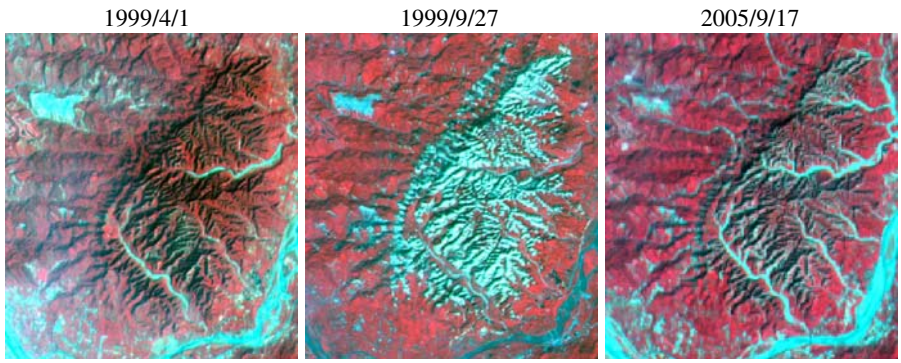

Fig. 2 SPOT satellite images at the Jou-Jou Mountain area

Methods

Three SPOT satellite images with 20-m pixels were used to identify post-quake landslides (Fig. 2). The first imagery was taken before the earthquake on April 1, 1999. The second imagery soon after the earthquake was on September 27, 1999. The third imagery was taken on September 17, 2005, over 6 years after the earthquake. The upper left corner is golf course in the studied image and some areas were undergoing vegetation works and had a positive change value.

Landslide image analysis

Landslide spectral characteristics

The SPOT imagery has green, red and near-infrared wavebands. In green and red wavebands, the landslide has a stronger reflectance (brightness) than vegetation and water land covers (Fig. 3). However, in the near-infrared waveband, vegetation can reflect the near-infrared stronger than water and landslide bare soil. Areas of bare soil from landslides, vegetation and water are major land covers distributed through the study area in post-quake images. In this study, a new evaluating index, the average brightness index (ABI), was proposed to substitute for near-infrared waveband. The ABI can be written as:

$$\mathrm{ABI} = \frac{(G + R + \mathrm{NIR})}{3} \tag{1}$$

where G is the reflectance radiated in the visible green waveband of the satellite radiometer, R is the reflectance radiated in the visible red waveband and NIR is the reflectance radiated in the near-infrared waveband. The ABI will have higher values (strong reflectances) for landslide areas.

Image differencing algorithm

Image differencing is based on a pair of coregistered images of the same area collected at different times. The process simply subtracts one digital image, pixel-

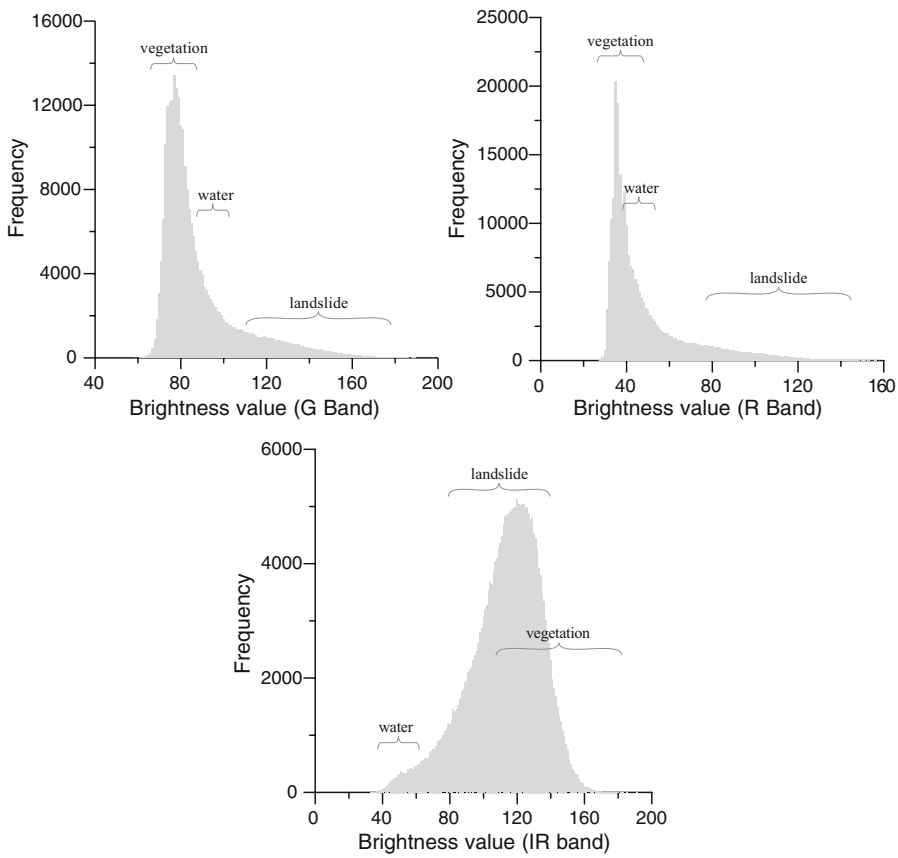

Fig. 3 The brightness frequency for major three land covers in post-quake image

by-pixel, from another, to generate a third image composed of the numerical differences between the pairs of pixels (Ridd and Liu 1998). The differenced image can be derived from pre- and post-quake images by applying the image differencing algorithm. In this study, the land cover change types were categorized by the method of image subtraction, brightness value after hazard subtracted from that before the hazard. The three major change types are positive change, no change and negative change. (1) Positive change has a differencing brightness value larger than 0 because vegetation is replacing bare land surface. (2) No change is the differencing brightness value close to 0, which suggest areas not affected by the hazard such as undamaged buildings, unchanged vegetated areas and bare land. (3) Negative change is the differencing brightness value smaller than 0, which indicates areas where denudation of vegetation cover has occurred since the time of the earthquake. In this study, the focus in on the recovery of denuded landslides caused the earthquake, hence, pixels with differencing brightness value smaller than 0 were excluded while performing landslide image analysis of vegetation recovery rates.

Landslide extraction using self-organizing map and fuzzy technique combined model

Self-organizing map neural network

The Self-organizing Map (SOM), originally proposed by Kohonen in 1997, is a popular feed-forward artificial neural network based on unsupervised learning, which has properties of both vector quantization and vector projection algorithms (Kohonen 1997). The network consists of an input layer and an output layer (also called the competitive layer; Fig. 4). The input layer is fully connected to the output layer. In SOM, the high-dimensional input vectors are projected in a nonlinear way to a low-dimensional map (usually a two-dimensional spaces), and SOM can perform this transformation adaptively in a topologically ordered fashion. Therefore, the neurons are placed at the nodes of a two-dimensional grid. Each neuron i has an associated d-dimensional prototype vector, $m_i = [m_{i1}, m_{i2}, ..., m_{id}]$, where d denotes the dimension of the input vectors.

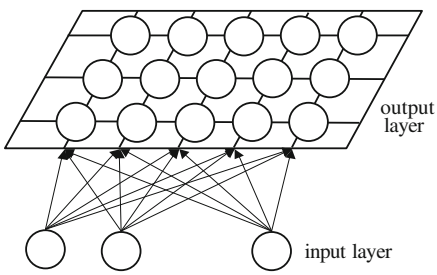

Fig. 4 The self-organizing map structure

The SOM is trained iteratively. In each training step, one sample vector x from the input data set is chosen randomly and the similarity between it and all prototypes of the map are calculated using the Euclidian distance measure. The unit whose incoming connection weights have the greater similarity with the input pattern x is the winner unit c (best matching unit, BMU):

$$\|x - m_c\| = \min_i\{\|x - m_i\|\} \tag{2}$$

where $\|\cdot\|$ is the Euclidian distance measure.

After finding the BMU, the prototype vectors (or connection weights) are adjusted. The SOM not only updated the BMU's weights, but also adjusted the weights of the adjacent output units in close proximity to the neighborhood of the winner. The update equation for applying the weight vector of neuron i is:

$$m_i(t+1) = m_i(t) + \alpha(t)h_{ci}(t)[x(t) - m_i(t)] \tag{3}$$

where t is the time of iteration, $\alpha(t)$ is the learning rate and is a decreasing function of time, $h_{ci}(t)$ is called the neighborhood function, which will decrease in time. The Gaussian function was used as the neighborhood function in this study:

$$h_{ci}(t) = \exp\left(-\frac{\|r_i - r_c\|^2}{2\sigma^2(t)}\right) \tag{4}$$

where $\sigma(t)$ is called the neighborhood radius; $\|r_i - r_c\|$ is the topological distance between unit i and winner unit c.

In this study, the dimension of the input vector is three because two wavebands, G and R, and one brightness index, ABI, in satellite image were chosen as the data sources. In SOM, the learning is broken down into two phases: the ordering phase and tuning phase. In the ordering phase, the neighborhood radius decreases linearly from 5 to 1, and the value of 1 was maintained over the tuning phase. The initial learning rates were 0.9 and 0.25, and the training lengths were

2,000 and 10,000 epochs for the ordering phase and tuning phase, respectively. The learning rate decreased linearly from 0.25 to zero during training in the tuning phase. Additionally, a rectangular grid with 81 (9×9) neurons was used in the Kohonen map. When the training is over, the map should be topologically ordered and similar input vectors can map to the same or adjacent neurons. Because landslides have larger brightness values in three input vectors, similar trend for the trained weight vectors can be found in the Kohonen map. The landslide land cover can be rapidly extracted based on the derived weight vectors. The larger the weight vectors, the higher the possibility of pixel belonging to the landslide. Therefore, the ordered weight vectors coupled with fuzzy technique can be used to rapidly identify post-quake denudation sites.

Landslide extraction using fuzzy technique

The GIS-based fuzzy classifier consists of a fuzzy *c*-mean algorithm and the geo-link technique of GIS. The former is a nonhierarchical clustering algorithm, which randomly assigns pixels to classes and then, in an iterative process, moves cases to other classes so as to minimize the generalized least-squared error (Bezdek 1981). The latter is a spatial link technique that displays the extracting results on a GIS platform, which are compared with ground truth or aerial photos. By the combination of GIS and fuzzy techniques, areas with landslides can be quickly extracted.

After training in SOM, the landslide has larger weight vectors in neurons. Therefore, the trained weight vectors can be divided into two classes. The first class is the landslide having larger weight values, and the second class is the non-landslide having smaller weight values. The larger the weight vectors, the higher the possibility of a pixel being a landslide. As a result, fixed cluster centers for two classes are assigned: $\max(W_G, W_R, W_{\mathrm{ABI}})$ for the first class and $\min(W_G, W_R, W_{\mathrm{ABI}})$ for the second class, in which W_G, W_R and W_{ABI} are the trained weight vectors of differenced *G*, *R* and ABI in SOM, respectively.

The fuzzy *c*-partition *U* of a given data set *Y* can be found by applying:

$$J_m(U,v) = \sum_{i=1}^{c}\sum_{j=1}^{n} \left(u_{ij}\right)^m \left\|y_j - v_i\right\|^2 \qquad (5)$$

where $Y = \{y_1, y_2, ..., y_n\} \subset R$=the data, c = the number of clusters identified, $2 \le c < n$, m = weighting exponent, $1 \le m < \infty$, U = fuzzy c-partition of Y, $U \subset M_{fc}$, u_{ij}=the degree of membership of pattern y_j in cluster v_i, $u_{ij} = \frac{1}{\sum_{k=1}^{c}\left(\left\|w_b y_j - v_i\right\|^2 / \left\|y_j - v_k\right\|^2\right)^{\frac{1}{m-1}}}$, v_i=$(v_1, v_2, \ldots, v_c)$=vectors of cluster centers, $v_i = \frac{\sum_{j=1}^{n}\left(u_{ij}\right)^m y_j}{\sum_{j=1}^{n}\left(u_{ij}\right)^m}$, $\|\|^2$= the Euclidean distance from a pattern y_j to the cluster center v_i.

After calculating fuzzy membership function for each neuron in SOM, areas of landslide can be rapidly identified according to membership values in descending order. Optimal threshold membership value decision for landslide extraction can be rapidly chosen from the neurons of output vector in SOM after compared with compared with ground truth data such as aerial photos or field surveys. The classification accuracy for the extracted landslides can be assessed using Kappa coefficient, which is a measure of agreement or accuracy for land cover classification (Congalton 1991).

Vegetation recovery rate assessment

The SPOT satellite image shows green, red and near-infrared as the three major wavebands. Because vegetation can reflect the near-infrared stronger than bare soil, this characteristic was used to investigate and explore the vegetation using its photosynthetic conditions. The normalized difference vegetation index (NDVI) is one of the most popular methods for vegetation monitoring. The NDVI calculation (Justice et al. 1985) can be obtained as:

$$\mathrm{NDVI} = \frac{\mathrm{NIR} - R}{\mathrm{NIR} + R}$$

where NIR is the reflectance radiated in the near-infrared waveband and *R* is the reflectance radiated in the visible red waveband of the satellite radiometer. The higher the NDVI value, the higher the photosynthesis activity. It has been reported that multi-temporal NDVI is useful for classifying land cover and dynamics of vegetation (Senay and Elliott 2000; Birky 2001; Tsai and Philpot 2002).

In this study, an NDVI-based index, the vegetation cover index (*C*) was inferred using remote sensing

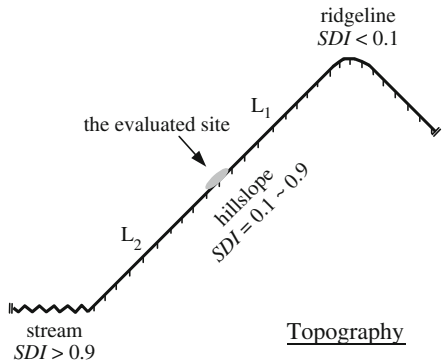

Fig. 5 Illustration of location analysis

combined with ground-truthing based on the verification for several Taiwan's watersheds (Lin 2002). The proposed vegetation cover index relating to NDVI can be expressed as:

$$C = \left(\frac{1 - \mathrm{NDVI}}{2}\right)^{1+\mathrm{NDVI}} \tag{7}$$

The C values range from 0 to 1. The lower the C value, the higher the vegetation cover. The variation in C values was used to explain the degree of vegeta-

(a) differenced G weight vector

-0.110	-0.170	-0.203	-0.222	-0.239	-0.264	-0.292	-0.320	-0.360
-0.068	-0.110	-0.144	-0.169	-0.196	-0.228	-0.260	-0.303	-0.347
0.089	0.086	0.031	-0.032	-0.088	-0.144	-0.189	-0.233	-0.286
0.428	0.399	0.240	0.075	-0.043	-0.119	-0.167	-0.219	-0.268
0.933	0.948	0.716	0.364	0.101	-0.035	-0.096	-0.139	-0.191
1.494	1.252	0.831	0.389	0.126	0.019	-0.035	-0.093	-0.149
2.033	1.773	1.332	0.807	0.420	0.210	0.103	0.021	-0.052
2.349	1.855	1.194	0.728	0.458	0.282	0.160	0.062	-0.008
2.811	2.413	1.602	0.956	0.650	0.453	0.291	0.176	0.084

(b) differenced R weight vector

-0.123	-0.169	-0.202	-0.227	-0.240	-0.245	-0.247	-0.248	-0.247
-0.074	-0.131	-0.180	-0.211	-0.227	-0.236	-0.243	-0.248	-0.249
0.060	0.021	-0.061	-0.132	-0.173	-0.200	-0.221	-0.236	-0.246
0.272	0.212	0.075	-0.043	-0.112	-0.161	-0.197	-0.222	-0.235
0.664	0.678	0.509	0.257	0.072	-0.034	-0.109	-0.163	-0.193
1.219	1.052	0.765	0.443	0.206	0.052	-0.056	-0.114	-0.131
1.847	1.640	1.331	0.934	0.559	0.283	0.100	-0.006	-0.053
2.336	1.934	1.389	0.887	0.528	0.284	0.133	0.040	-0.023
2.913	2.551	1.849	1.151	0.709	0.430	0.259	0.148	0.052

(c) differenced *TBI* weight vector

0.590	0.390	0.270	0.179	0.091	-0.010	-0.117	-0.220	-0.315
0.434	0.309	0.210	0.116	0.015	-0.093	-0.199	-0.314	-0.407
0.496	0.390	0.265	0.146	0.037	-0.069	-0.175	-0.300	-0.444
0.563	0.434	0.254	0.096	-0.023	-0.135	-0.258	-0.416	-0.534
0.873	0.788	0.566	0.295	0.086	-0.063	-0.195	-0.338	-0.471
1.276	1.046	0.700	0.327	0.054	-0.119	-0.256	-0.383	-0.469
1.892	1.633	1.220	0.690	0.234	-0.035	-0.190	-0.321	-0.437
2.372	1.851	1.109	0.463	0.076	-0.135	-0.288	-0.426	-0.519
3.001	2.548	1.623	0.727	0.210	-0.066	-0.252	-0.404	-0.509

Fig. 6 The weight vectors mapped on the Kohonen maps

tion recovery at landslides from pre- and post-quake satellite images. The rate of vegetation recovery (v) can be written as:

$$v(\%) = \frac{C_1 - C_2}{C_1 - C_0} \times 100\% \quad (8)$$

where C_0 is the pre-quake vegetation cover index; C_1 is the vegetation cover index soon after the earthquake; and C_2 is the vegetation cover index at the time of assessment. The values for vegetation recovery v were grouped into four categories, including poor (<0), average (0–50), good (50–100), and excellent (>100). Based on v values, three conditions can be obtained: (1) Vegetation recovery became worse if v is less than 0; (2) Vegetation recovery is gradually enriched if v ranged from 0 to 100; (3) Vegetation recovery is superior to that before the earthquake if v is greater than 100.

Vegetation recovery pattern analysis

The Jou-Jou Mountain area was chiefly formed by high percentage of gravel and rock. A unique cliff terrain resulted from this geomorphic activity, which caused special vegetation recovery pattern at the post-quake landslides. Due to the differences among topographic characteristics, plant formation and soil moisture, three main vegetation recovery patterns were observed from field surveys, including the invading pattern, the surviving pattern and the mixed pattern. The invading pattern, located near gentle toe-slopes along stream, can preserve sufficient water in the topsoil for establishing pioneer plants. The surviving pattern, located along steep slope, is unstable and the plants cannot readily attach to the surface. Therefore, the denudation sites were recovered on the basis of the original surviving vegetation. The mixed pattern is located on ridgelines having insufficient soil moisture. The vegetation cover is a mix of original and invading plants.

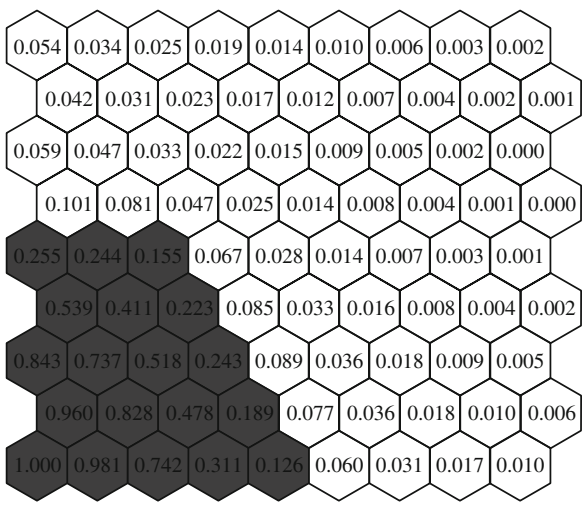

Fig. 7 The calculated fuzzy membership function mapped on the Kohonen maps

Fig. 8 Landslide distribution at the Jou-Jou Mountain area

In order to assess the location of different vegetation recovery patterns on landslides, an evaluating index, the spatial distribution index (SDI), was developed to calculate land-cover distribution, including on ridgeline, along hillslope and near stream (Fig. 5) from upstream source to downstream area. The SDI formula can be expressed as:

$$\mathrm{SDI} = \frac{L_1}{L_1 + L_2} \quad (9)$$

where L_1 is the distance from the evaluated site to the ridgeline, and L_2 is the distance from the evaluated site to the stream. By GIS analysis, both distances can be derived from DEMs using site position and calculated drainage flow direction. The required terrain data, such as drainage flow direction and drainage network, can be automatically derived by using the algorithms proposed by Chou et al. (2004) and Lin et al. (2006).

The SDI value ranges from 0 to 1. If the value is close to 1, the evaluated site is near a stream. If the value ranges from 0.1 to 0.9, the evaluated site is located on the hillslope. If the value is close to 0, the evaluated site is located on the ridgeline.

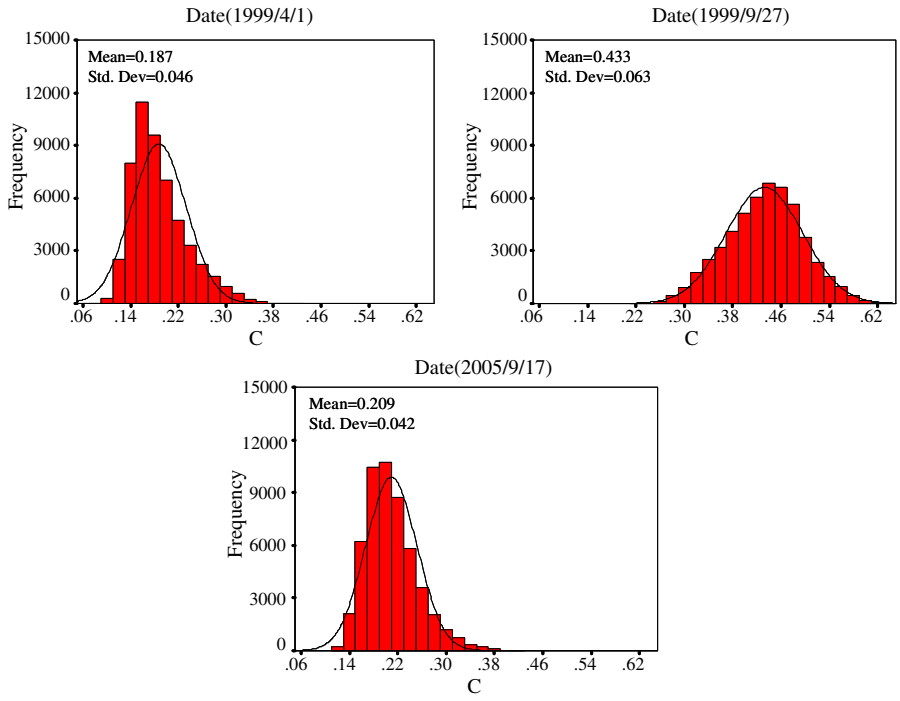

Fig. 9 Frequency distribution of vegetation cover index (*C*) in the denudation sites

Results and discussion

Landslide extraction and topographic characteristics

In accordance with the geological data from Taiwan's Central Geological Service, the geology of study area was chiefly formed by high percentage of gravel, rock and minor sandstone. The surface was only covered by shallow and fragile topsoil. It would be collapsed and cause large-scale scattered landslides during catastrophic earthquakes. The SPOT imagery on September 27, 1999, about 1 week after the earthquake, shows that much of standing vegetation was eliminated, and massive landslides are widely distributed throughout the study area (Fig. 8).

Three input vectors, the differenced *G*, *R* and ABI, can be transferred as weight vectors after iteratively training in SOM and the converged weight vectors

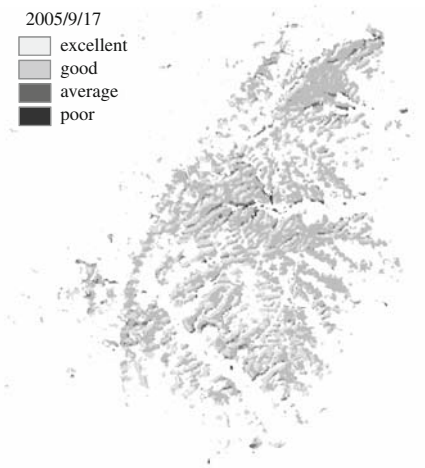

Fig. 10 Spatial distribution of classified *v* in the denudation sites

Fig. 11 Scoured slope bases next to the concave banks of river

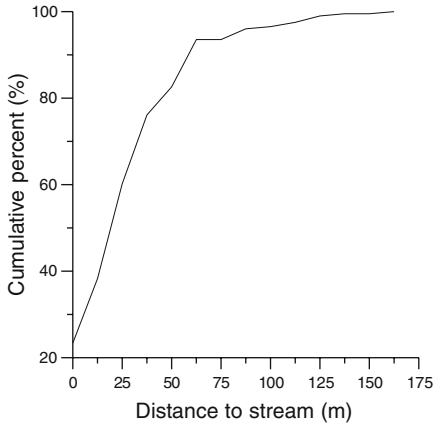

Fig. 12 The distance analysis of the poor vegetation recovery sites

mapped on a Kohonen map (Fig. 6). SOM is a useful tool for the visualization of association of similar land covers distribution, and with the help of Kohonen map, the associations of similar land covers can be observed very clearly. In accordance with high reflectance characteristic of the landslide, the larger the pixel brightness value, the higher the possibility belonging to the landslide. The weight vector trained in SOM has the same association with the darker color represents larger weight value; that is, higher possibility belonging to the landslide. Based on the distribution of trained weight vectors, the landslide soon after the earthquake (1999/9/27) was concentrated near the lower-left side of neurons.

When the training process was finished and the prototype vectors were obtained, fuzzy technique was utilized to calculate fuzzy membership function of neurons of the SOM. The larger the membership function value of neurons, the higher the possibility of pixel belonging to the landslide. The fuzzy membership function of neurons for post-quake images was calculated (Fig. 7), and compared with ground truth data such as aerial photos and field survey, the minimum threshold of fuzzy membership function for landslide extraction on September 27, 1999 is 0.126. Pixels greater than the threshold were identified as landslide (Fig. 8). The extracted landslide area was 849.20 ha with a high Kappa coefficient of 0.9453.

The topographic characteristics of the landslide sites can be calculated on the basis of location analysis. The percentages of the landslide distributed on ridgeline, along steep slope and near stream are 45.13%, 50.34% and 4.52%. The steep sites on ridgeline and along steep slope belong to the collapsed area of the landslide, with worse environmental conditions for plants growing, including bare gravel and rock, infertile collapsed land and insufficient soil moisture. The sites with gentle slope near stream belong to the heap area of the landslide, with gentler slope and sufficient soil moisture for plants growing.

Vegetation recovery pattern assessment

The *C* frequency distribution for sites before the Chi-Chi earthquake indicates excellent vegetation condition with an average *C* value of 0.187 (Fig. 9), but much of the vegetation was eliminated soon after the earthquake as indicated by an average *C* value of 0.433. After 6 years of monitoring, the average *C* value has declined to 0.209 on September 17, 2005, indicating that vegetation on landslides has been gradually recovered by 86%.

Most poor recovery sites were spatially distributed along stream banks (Fig. 10), which was verified by

Table 1 Statistics of classified vegetation recovery conditions at different dates

Category	*v* (%)	Distribution by date (2005/9/17)			
		Near stream	Along hillslope	On ridgeline	Total
Area in hectare (%)					
Excellent	>100	6.05 (0.71)	144.41 (17.01)	136.56 (16.08)	287.02 (33.80)
Good	50~100	25.31 (2.98)	254.66 (29.99)	239.47 (28.20)	519.44 (61.17)
Average	0~50	6.54 (0.77)	19.59 (2.31)	13.36 (1.57)	39.49 (4.65)
Poor	<0	0.76 (0.09)	2.31 (0.13)	1.36 (0.16)	3.25 (0.38)
Total		38.66 (4.55)	419.79 (49.44)	390.75 (46.01)	849.20 (100)
Average *v*		71.32%	85.97%	87.42%	85.96%

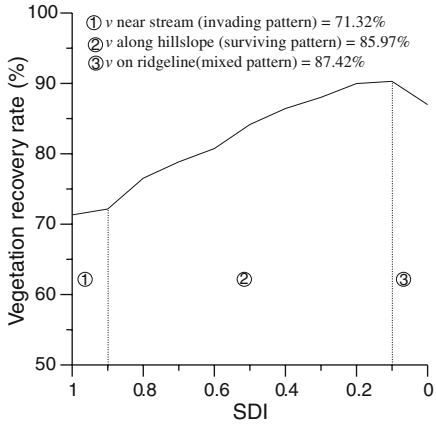

Fig. 13 Vegetation recovery rate for three patterns

Fig. 15 The restoring *Arundo formosana* Hack on steep slopes (2005/8)

field surveys. The reason is that scoured slope bases next to the concave banks of river were easily eroded during rainfall seasons (Fig. 11). The distance analysis from poor recovery sites to stream indicates that up to 82.59% of poor sites concentrated around stream banks with distance less than 50 m (Fig. 12). Additionally, from 1999 through 2005, several typhoons, such as Toraji (2001/7/30), Mindulle (2004/7/2), Aere (2004/8/25) and (2005/7/18), have stroke the Jou-Jou Mountain area and caused debris flow disasters. The assessed results show that the impact on vegetation recovery at landslides is insignificant and the nature itself has strong vegetation recovery ability for the denudation sites.

In accordance with vegetation recovery pattern assessment, the v values for the sites of invading, surviving and mixed patterns are 71%, 86% and 87%, respectively (Table 1). It is obvious that the vegetation recovery declined along landforms from ridgeline to stream (Fig. 13) with on ridgelines and along steep slopes having superior vegetation recovery than sites near streams. Three vegetation recovery patterns were analyzed and described as follows:

1. The invading pattern is mainly located at gentle toe-slopes near stream, where sufficient water is preserved in topsoil for native pioneer plants to establish. The dominated plants include *Rhus chinesis*, *Mallotus Japonicus*, *Broussonetia papyrifera*, *Trema orientalis* and *Miscanthus floridulus*. They are the commonly found pioneer plants

Fig. 14 The vegetated buffer strips formed by the invading pioneer plants (2005/8)

Fig. 16 The surviving *Pinus taiwanensis* Hayata and invading vegetation on ridgeline (2005/8)

on infertile collapsed lands in Taiwan. The seeds of pioneer plants with lighter weights could be transported to the denudation sites at gentle slopes via wind power from other areas. From field observations, once sufficient water supplied, they can rapidly grow, and expand as stable plant communities within three years. Those natural vegetated buffer strips protect the collapsed earth and stones from being eroded (Fig. 14). Additionally, because the scoured slope bases next to the concave banks caused unstable vegetation condition during rainfall seasons, the sites might need foundation engineering at first to establish a stable habitat for plants.

2. The surviving pattern occurs along steep hillslope because the invading seeds cannot be attach on the surface in the cliffs. The vegetation remains simple and composed mainly of the original surviving vegetation, especially *Arundo formosana* Hack (Fig. 15), one of the native grass species with robust vitality in Taiwan. *Arundo formosana* is a pioneer plant that can survive in harsh environments, such steep cliff, which typically have insufficient soil moisture and infertile topsoil. Due to its robust rootstalk, it can subsist and rapidly grown along steep collapsed slopes during rainfall seasons. The tendency of vegetation to recover increased from slope surface to ridgeline. Over six years of natural succession, most collapsed slopes have recovered. Our results indicate that slope gradient is not a limiting environment factor for vegetation recovery on landslides.
3. The mixed pattern is located on ridgelines where there is often insufficient soil moisture for plant growth. The vegetation cover is mainly *Arundo formosana* and trees such as *Pinus taiwanensis* Hayata and *Pinus morrisonicola* Hayata (Fig. 16). The *Pinus taiwanensis* not only can endure drought environments but can also develop mycorrhiza symbiosis. These pines obtain enough nitrogen and other essential minerals from humus decomposition, aided on mycorrhiza functions. Meanwhile, the plants provide carbohydrate and amino acid to support the mycorrhiza. The invading plants mainly consist of *Mallotus japonicus*, *Macaranga tanarius* and *Miscanthus floridulus*, whose seeds endure long-term droughts on ridgelines and wait for rains.

Conclusions

Assessment of landslide hazard and monitoring its vegetation recovery is an important task for decision making and policy planning in landslide prone area. We evaluated three methods for assessing the occurrence of landslides and their vegetation recovery, including a combined SOM neural network and fuzzy technique, a NDVI-based vegetation recovery index, and a spatial distribution index. After six years of natural succession, excellent vegetation recovery had occurred on landslides. Based on field surveys, the original surviving plants with robust vitality played a vital role in the process of natural vegetation succession in the Jou-Jou Mountain study area. During rainy seasons, landslides can rapidly recover to protect fragile lands from being eroded and avoiding debris flow disasters. Additionally, most poor vegetation recovery sites were mainly distributed at scoured slope bases next to the concave stream banks, which might need initial engineering to establish a stable habitat for plant establishment.

References

Andrefouet, S., Roux, L., Chancerelle, Y., & Bonneville, A. (2000). A fuzzy possibilistic scheme of study for objects with indeterminate boundaries: Application to French Polynesian reefscapes. *IEEE Transactions on Geoscience and Remote Sensing*, *38*, 257–270.

Bezdek, J. C. (1981). *Pattern recognition with fuzzy objective function algorithms*. New York: Plenum.

Birky, A. K. (2001). NDVI and a sample model of deciduous forest seasonal dynamics. *Ecological Modelling*, *143*, 43–58.

Brown, G., & Al-Mazrooei, S. (2003). Rapid vegetation regeneration in a seriously degraded *Rhanterium epapposum* community in northern Kuwait after 4 years of protection. *Journal of Environmental Management*, *68*, 387–395.

Carrara, A., Guzzetti, F., Cardinali, M., & Reinchenbach, P. (1999). Use of GIS technology in the prediction and monitoring of landslide hazard. *Natural Hazards*, *20*, 117–135.

Chang, C. C. (2000). *Using remotely sensed data for hillslope disasters assessment in the Chi-Chi earthquake. Seminar on the 921 Earthquake-induced Hillslope Disasters for Policy Planning*, Taichung, Taiwan, pp.32–41 (in Chinese with English abstract).

Chou, T. Y., Lin, W. T., Lin, C. Y., Chou, W. C., & Huang, P. H. (2004). Application of the PROMEHEE technique to determine depression outlet location and flow direction in DEM. *Journal of Hydrology*, *287*, 49–61.

Claessens, L., Verburg, P. H., Schoorl, J. M., & Veldkamp, A. (2006). Contribution of topographically based landslide

hazard modelling to the analysis of the spatial distribution and ecology of Kauri (*Agathis australis*). *Landscape Ecology*, *21*, 63–76.

Congalton, R. G. (1991). A review of assessing the accuracy of classification of remotely sensed data. *Remote Sensing of Environment*, *37*, 35–46.

Dhakal, A. S., Amada, T., & Aniya, M. (2000). Landslide hazard mapping and its evaluation using GIS: an investigation of sampling schemes for a grid-cell based quantitative method. *Photogrammetric Engineering and Remote Sensing*, *66*, 981–989.

Dikau, R., Cavallin, A., & Jager, S. (1996). Databases and GIS for landslide research in Europe. *Geomorphology*, *15*, 227–239.

Justice, C. O., Townshend, J. R. G., Holben, B. N., & Tucker, C. J. (1985). Analysis of the phenology of global vegetation using meteorological satellite data. *International Journal of Remote Sensing*, *6*, 1271–1318.

Keuchel, J., Naumann, S., Heiler, M., & Siegmund, A. (2003). Automatic land cover analysis for Tenerife by supervised classification using remotely sensed data. *Remote Sensing of Environment*, *86*, 530–541.

Kohonen, T. (1997). *Self-organizing maps*. Berlin: Springer.

Kumar, L., Rietkerk, M., Van Langevelde, F., Van De Koppel, J., Van Andel, J., Hearne, J., et al. (2002). Relationship between vegetation growth rates at the onset of the wet season and soil type in the Sahel of Burkina Faso: implications for resource utilisation at large scales. *Ecological Modelling*, *149*, 143–152.

Larchevêque, M., Montès, N., Baldy, V., & Dupouyet, S. (2005). Vegetation dynamics after compost amendment in a Mediterranean post-fire ecosystem. *Agriculture Ecosystems & Environment*, *110*, 241–248.

Lin, W. T. (2002). *Automated watershed delineation for spatial information extraction and slopeland sediment yield evaluation*. PhD dissertation, National Chung Hsing University, Taiwan (in Chinese with English abstract).

Lin, W. T., Chou, W. C., Lin, C. Y., Huang, P. H., & Tsai, J. S. (2006). Automated suitable drainage network extraction from digital elevation models in Taiwan's upstream watersheds. *Hydrological Processes*, *20*, 289–306.

Lin, H. H., & Huang, C. J. (2000). Vegetation engineering treatment at landslides after the Chi-Chi earthquake. *Proceedings of the Second National Conference on Landslide Stabilization and Disaster Prevention Research in Taiwan*, Taipei, Taiwan, pp. 23–36 (in Chinese with English abstract).

Lin, C. Y., Wu, J. P., & Lin, W. T. (2001). The priority of revegetation for the landslides caused by the catastrophic Chi-Chi earthquake at Ninety-nine Peaks in Nantou area. *Journal of Chinese Soil and Water Conservation*, *32*, 59–66 (in Chinese with English abstract).

Mantovani, F., Soeters, R., & Van Westen, C. J. (1996). Remote sensing technique for landslide studies and hazard zonation in Europe. *Geomorphology*, *15*, 213–225.

Myster, R. W., Thomlinson, J. R., & Larsen, M. C. (1997). Predicting landslide vegetation in patches on landscape gradients in Puerto Rico. *Landscape Ecology*, *12*, 299–307.

Ou, C. H., & Liu, C. C. (2000). Investigation of native vegetation on the landslide caused by the 921 Earthquake. *Seminar on Vegetation Engineering for Soil and Water Conservation*, Taichung, Taiwan, pp.15–23 (in Chinese with English abstract).

Perotto-Baldiviezo, H. L., Thurow, T. L., Smith, C. T., Fisher, R. F., & Wu, X. B. (2004). GIS-based spatial analysis and modeling for landslide hazard assessment in steeplands, southern Honduras. *Agriculture Ecosystems & Environment*, *103*, 165–176.

Ridd, M. K., & Liu, J. (1998). A comparison of four algorithms for change detection in an urban environment. *Remote Sensing of Environment*, *63*, 95–100.

Roovers, P., Bossuyt, B., Gulinck, H., & Hermy, M. (2005). Vegetation recovery on closed paths in temperate deciduous forests. *Journal of Environmental Management*, *74*, 273–281.

Sellers, P. J. (1985). Canopy reflectance, photosynthesis and transpiration. *International Journal of Remote Sensing*, *6*, 1335–1372.

Senay, G. B., & Elliott, R. L. (2000). Combining AVHRR-NDVI and landuse data to describe temporal and spatial dynamics of vegetation. *Forest Ecology and Management*, *128*, 83–91.

Teillet, P. M., Staenz, K., & Williams, D. J. (1997). Effects of spectral, spatial, and radiometric characteristics on remote sensing vegetation indices of forested regions. *Remote Sensing of Environment*, *61*, 139–149.

Tsai, F., & Philpot, W. D. (2002). A derivative-aided hyperspectral image analysis system for land-cover classification. *IEEE Transactions on Geoscience and Remote Sensing*, *40*, 416–425.

Wang, W. N., Chigira, M., & Furuya, T. (2003). Geological and geomorphological precursors of the Chiu-fen-erh-shan landslide triggered by the Chi-Chi earthquake in central Taiwan. *Engineering Geology*, *69*, 1–13.

Wang, W. N., Yin, C. Y., Chen, C. C., & Lee, M. C. (2000). *Distribution and characteristics of slope failures induced by 921-earthquake in central Taiwan. Researches on Mountain Disasters and Environmental Protection across Taiwan Strait (II)*, Taipei, Taiwan, pp.223–233 (in Chinese with English abstract).